with the γ decay of the 3.65- and 3.68-MeV states,[6] but we have no such information on the 4.23-MeV state. The spectroscopic factors for these states are small, however, and the values are not significant in the calculations. Incorrect assignments would only slightly alter the quoted percentages. We also show in Table V the results of similar calculations[18,19] for Si^{28}. In this case, the spins of the Al^{27} levels are well known,[2] and ambiguities of the kind experienced in this work were not encountered. Both experiments, however, investigate the closure of the $1d_{5/2}$ proton shell, and we expect the occupation numbers to be similar.

If we assume the 3.07-MeV state to be $\frac{5}{2}^+$, then the $1d_{3/2}$ and $2s_{1/2}$ shells have approximately equal populations, the same as is observed for Si^{28} as shown in columns 4 and 5 of Table V. The upper $1d_{3/2}$ limit shown in column 5 must be treated with reserve as Wildenthal and Newman[19] were unable to resolve the $\frac{3}{2}^+$ state at 2.976 MeV in Al^{27} from a $\frac{9}{2}^+$ state at 3.001 MeV. Their spectroscopic factor was extracted after fitting a combination of $l=2+4$ to the observed doublet distribution. Gove *et al.*[18] show that such a procedure is far from rigorous as the 3.001-MeV state, similarly formed in their experiment, did not show a pattern that could be reconciled with an $l=4$ distorted wave fit.

In view of these results, as well as the fact that the ground states of Si^{29} and P^{29} have $J^\pi=\frac{1}{2}^+$, indicating that in this region the $2s_{1/2}$ shell is lower in energy than the $1d_{3/2}$, it is unlikely that the occupation of the $1d_{3/2}$ shell would be four times that of the $2s_{1/2}$ shell which would be the case if the 3.07-MeV state had $J^\pi=\frac{3}{2}^+$. Faced with this evidence, we conclude that a $J^\pi=\frac{5}{2}^+$ assignment is favored for the 3.07-MeV level.

Two possible $l=3$ transitions have been observed in the energy region covered in the present experiment. We are unable to distinguish between the spin parity possibilities of $\frac{5}{2}^-$ and $\frac{7}{2}^-$, but the strength of these states is 4% of the total. We can regard this as an upper limit on the $(1f_{7/2})^2$ proton configuration in the Si^{30} ground state.

[18] H. E. Gove, K. H. Purser, J. J. Schwartz, W. P. Alford, and D. Cline, Nucl. Phys. **A116**, 369 (1968).
[19] B. H. Wildenthal and E. Newman, Phys. Rev. **167**, 1027 (1968).

ACKNOWLEDGMENTS

I would like to express my appreciation to Dr. J. A. Becker and Dr. J. C. Hardy for valuable discussions, Dr. R. N. Glover for arranging a successful exposure of the nuclear plates, and Miss Angela Eshleman for scanning the plates and partly processing these data.

PHYSICAL REVIEW VOLUME 180, NUMBER 4 20 APRIL 1969

Spin Flip in the Inelastic Scattering of Protons*†

W. A. Kolasinski,‡ J. Eenmaa,§ F. H. Schmidt, H. Sherif,|| and J. R. Tesmer
Department of Physics, University of Washington, Seattle, Washington 98105

(Received 23 December 1968)

Proton spin-flip probabilities and differential inelastic scattering cross sections were measured over a large angular region for the following 2^+ excitations: 4.44 MeV in ^{12}C at 12, 13, 14, 15, and 20 MeV; 1.45 MeV in ^{58}Ni at 9.25, 10.46, 15, and 20 MeV; 1.33 MeV in ^{60}Ni at 10.5 and 14 MeV; and 1.34 MeV in ^{64}Ni at 10.5 and 14 MeV. The results were analyzed in the distorted-wave Born approximation, with collective-model form factors derived from the optical-model potential. The deformed spin-dependent part of the coupling potential was of the full Thomas form, and the data are best described when $\beta_2^{SO}>\beta_2$. Good fits are obtained for elastic polarization data (obtained elsewhere) when the depth of the spin-orbit potential is determined from spin-flip probability measurements.

I. INTRODUCTION

NUMEROUS experiments involving the scattering of polarized protons have been performed in order to investigate spin-dependent forces in nuclei.[1-3] An alternative and complementary approach, and one which seems particularly attractive since it does not require the use of a polarized beam, is the measurement of spin flip in the inelastic scattering of protons from even-even nuclei. The method has been described in a

* Research supported in part by the U.S. Atomic Energy Commission.
† Portions of this work were submitted by one of us (W.A.K.) in partial fulfillment of the requirements for the Ph.D. degree at the University of Washington.
‡ Present address: Aerospace Corp., Los Angeles, Calif.
§ Supported in part by a National Science Foundation Traineeship grant.
|| Present address: University of Manchester, Manchester, England.

[1] *Proceedings of the Second International Symposium on Polarization Phenomena of Nucleons, Karlsruhe, 1965*, edited by P. Huber and H. Schopper (Birkhauser Verlag, Basel, Germany, 1966).
[2] M. P. Fricke, E. E. Gross, and A. Zucker, Phys. Rev. **163**, 1153 (1967).
[3] C. Glashausser, R. de Swiniarski, J. Thirion, and A. D. Hill, Phys. Rev. **164**, 1437 (1967). This and Refs. 1 and 2 contain many references to earlier work.

previous paper.[4] Results of measurements, performed with protons from the University of Washington Cyclotron at energies around 10.5 MeV on ^{12}C, ^{24}Mg, and ^{58}Ni, showed that the spin-flip probability attained values as high as 40%. The measurements also showed strong energy dependence, indicative of the dominant role played by compound-nuclear effects in the scattering mechanism at this energy. Although the method appeared promising as a tool for study of reaction mechanisms through measurement of substate populations, the cyclotron was found unsuitable due to the inherently poor duty cycle[5] and essentially fixed energy. Hence, further work was postponed pending the completion of an FN tandem Van de Graaff accelerator.[6] In this paper we present results of spin-flip measurements performed with the use of this accelerator, portions of which have been published in preliminary form.[7]

Calculations in the distorted-wave Born-approximation (DWBA) collective-model extension of the optical model, which have proved quite successful in reproducing cross-section and asymmetry measurements in inelastic scattering of protons at intermediate energies,[2,3,8–12] have recently been performed to obtain predictions of spin-flip probabilities.[13–18] This treatment gives a good account of spin-flip measurements at higher energies,[1,3,18] and it is found that spin-flip predictions are sensitive to the form of the deformed spin-dependent potential.[13,14,18]

II. EXPERIMENTAL METHOD

A. General Remarks

The theoretical basis of our method for measuring the spin-flip probability has been discussed in detail in Refs. 4 and 19. Briefly, the method is as follows. The angular-momentum quantization axis is chosen to be perpendicular to the scattering plane. The spin-flip probability is defined as the ratio of the number of protons scattered at a given angle with $\Delta\mu=\pm1$, to the total number of protons scattered at the same angle ($\Delta\mu=0,\pm1$), leaving the nucleus in a particular excited state. The quantity μ is the proton spin projection along the specified quantization axis. By application of a theorem due to Bohr[20] to the case where an even-even nucleus is left in a 2^+ excited state, one finds that the $m=\pm1$ nuclear substates can be excited if and only if $\Delta\mu=\pm1$, whereas for $\Delta\mu=0$, only the $m=0$ and the $m=\pm2$ substates can be populated. When the excited nuclei return directly to the ground state by electric-quadrupole ($E2$) γ-ray emission, only the $m=\pm1$ substates contribute to the γ-ray flux along the quantization axis. Thus, by placing a γ-ray detector along this axis and measuring the $(p, p'\gamma)$ correlation function, one can determine the probability for spin flip, provided the absolute efficiency of the γ-ray detector is known. The spin-flip probability (S) in inelastic scattering, where 2^+ states are excited, is given by the expression

$$S=\frac{8\pi}{5}\left[\frac{d^2\sigma}{d\Omega_\gamma d\Omega_p}\right]\Big/\frac{d\sigma}{d\Omega_p}, \qquad (1)$$

where $d^2\sigma/d\Omega_\gamma d\Omega_p$ is the double-differential cross section with γ rays emitted along the normal to the scattering plane, and $d\sigma/d\Omega_p$ is the ordinary inelastic differential cross section. It should be stressed that the above conclusions follow solely from conservation of parity and angular momentum, and the properties of electromagnetic radiation; they are therefore entirely independent of any specific reaction models.

Although the main features of the experiment are the same as described earlier,[4] numerous modifications and improvements were made to the equipment to facilitate the acquisition and reduction of the data.

B. Scattering Chamber and Detectors

The proton beam, the energy spread of which was approximately 1 keV, was focused onto a target located at the center of a 60-in.-diam scattering chamber. A 3-mm-diam defining aperture for beam alignment was located 15 cm upstream from the target. It could be introduced and withdrawn by remote control. A transmission >90% was obtained through the removable aperture. During data collection, no beam-defining apertures were used, in order to minimize background in the γ-ray detector, but beam alignment and focus were frequently checked by means of the remotely-controllable aperture. After passing through the target, the beam was stopped in a Faraday cup located about 100 cm from the scattering chamber exit port.

[4] F. H. Schmidt, R. E. Brown, J. B. Gerhart, and W. A. Kolasinski, Nucl. Phys. **52**, 353 (1964).
[5] F. H. Schmidt, H. Fauska, and J. W. Orth, *Nuclear Electronics III* (International Atomic Energy Agency, Vienna, 1962), p. 381.
[6] Provided by a National Science Foundation Grant.
[7] J. R. Tesmer, J. Eenmaa, and F. H. Schmidt, Bull. Am. Phys. Soc. **13**, 884 (1968); W. A. Kolasinski, J. G. Cramer, and F. H. Schmidt, *ibid.* **12**, 921 (1967); F. H. Schmidt, W. A. Kolasinski, and J. G. Cramer, *ibid.* **11**, 751 (1966); F. H. Schmidt, J. G. Cramer, and W. A. Kolasinski, *ibid.* **11**, 99 (1966); W. A. Kolasinski, J. G. Cramer, and F. H. Schmidt, *ibid.* **11**, 100 (1966).
[8] M. P. Fricke and G. R. Satchler, Phys. Rev. **139**, B567 (1965).
[9] S. F. Eccles, H. F. Lutz, and V. A. Madsen, Phys. Rev. **141**, 1067 (1966).
[10] M. P. Fricke, R. M. Drisko, R. H. Bassel, E. E. Gross, B. J. Morton, and A. Zucker, Phys. Rev. Letters **16**, 746 (1966).
[11] D. J. Baugh, M. J. Kenney, J. Lowe, D. L. Watson, and H. Wojciechowski, Nucl. Phys. **A99**, 203 (1967).
[12] S. A. Fulling and G. R. Satchler, Nucl. Phys. **A111**, 81 (1968).
[13] R. O. Ginaven, E. E. Gross, J. J. Malanify, and A. Zucker, Phys. Rev. Letters **21**, 552 (1968).
[14] H. Sherif and J. S. Blair, Phys. Letters **26B**, 489 (1968).
[15] B. Ballini, N. Cindro, J. Delauney, J. Fouan, M. Loret, and J. P. Passerieux, Nucl. Phys. **A97**, 561 (1967).
[16] D. M. Patterson and J. G. Cramer, Phys. Letters **27B**, 373 (1968).
[17] F. G. Perey, in *Proceedings of the Second International Symposium on Polarization Phenomena of Nucleons, Karlsruhe, 1965*, edited by P. Huber and H. Schopper (Birkhausser Verlag, Basel, Germany, 1966), p. 191.
[18] J. Eenmaa, F. H. Schmidt, and J. R. Tesmer, Phys. Letters **28B**, 321 (1968).
[19] W. A. Kolasinski, Ph.D. thesis, University of Washington, 1967 (unpublished).
[20] A. Bohr, Nucl. Phys. **10**, 486 (1959).

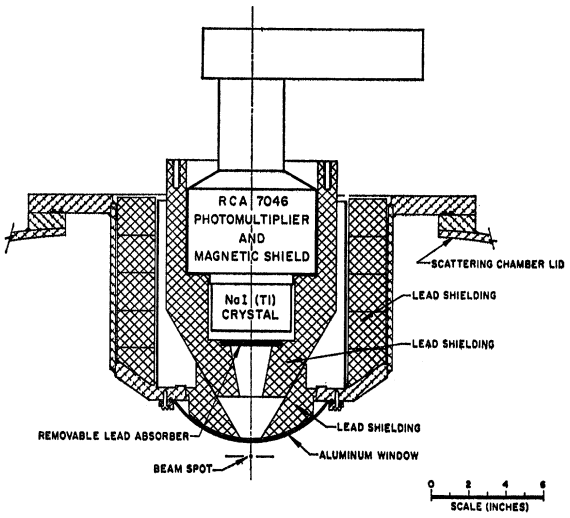

FIG. 1. Cross section of γ-ray detector shielding and support-well assembly.

The beam-disposal tube and Faraday cup were surrounded by a large neutron and γ-ray shield,[21] which served to reduce beam-induced background in the γ-ray detector.

A special assembly in the form of a well, shown in Fig. 1, was mounted at the center of the dome-shaped scattering chamber lid and served to support the γ-ray detector and lead shielding. The detector itself consisted of a 4×4-in. NaI(Tl) crystal mounted on an RCA 7046 photomultiplier tube. The half-angle subtended at the beam-spot position by the γ-ray detector in the lead shield was 11°. To reduce the flux of low-energy γ rays entering the detector, a $\frac{1}{8}$-in.-thick lead absorber was placed in front of the crystal.

Proton detectors, mounted on movable arms inside the scattering chamber, were placed at a distance of 15.4 cm from the target. Initially, a single surface-barrier detector was used in the correlation measurements. Subsequently, in order to decrease the data-collection time, two lithium-drifted silicon detectors were used on opposite sides of the beam. These detectors were cooled with liquid nitrogen to increase the signal-to-noise ratio in the time pickoff units.[22] Another particle detector was used as a fixed-angle beam-intensity monitor.

The anode signals from the γ-ray detector were limited, differentiated, and used for coincidence timing. Integrated pulses for energy discrimination were obtained from the tenth dynode. Fast-rise (10 nsec) differentiated pulses from the particle detectors, for coincidence timing, were obtained by the transformer-coupling technique described by Williams and Biggerstaff.[23] Charge from the detector passed through the transformer primary to a charge-sensitive preamplifier. Both the fast and charge-sensitive preamplifiers were mounted near the detector, in vacuum, in order to minimize stray noise pickup. Energy resolution obtained with this system was around 50 keV.

C. Targets

All targets were thin, self-supporting foils mounted on aluminum frames. The carbon targets consisted of 0.00075-in.-thick polystyrene sheets. The nickel-isotope foils were prepared by electroplating the nickel onto a thin copper backing and the copper was subsequently etched away. Material for the nickel targets was obtained from the Oak Ridge National Laboratory. The quoted isotopic enrichments were 99.9%, 99.8%, and 98.2% for ^{58}Ni, ^{60}Ni, and ^{64}Ni, respectively. Each of these targets had a surface density of approximately 1 mg/cm^2, with an estimated uncertainty of ~10%.

D. Electronic System

A conventional fast-slow coincidence arrangement with a resolving time of 20–30 nsec was used. Leading-edge timing was employed, with the fast proton pickoff signals and fast γ signals driving tunnel-diode discriminators. Output signals from the discriminators were routed through variable delays to the inputs of a fast coincidence unit. In the later phase of this work, the fast coincidence unit was replaced by a time-to-amplitude converter followed by a single-channel pulse analyzer whose window was set to encompass the coincidence peak [typically about 4 nsec full width at half-maximum (FWHM)]. This system greatly facilitated the over-all alignment of the circuit and the evaluation of the coincidence efficiency, which was determined to be 100% for pulses exceeding the slow discriminator thresholds.

The integrated signals from the proton detectors were passed through a biased amplifier so that only the elastic and first-inelastic proton groups were analyzed. Noncoincidence spectra of protons as well as those gated by the coincidence system (proton and γ energies and the p-γ time difference) were simultaneously stored in different portions of the analyzer memory. In the later stages of the work, the γ and proton energy pulses were routed to analog-to-digital converters, which provided the interface to a Scientific Data Systems 930 computer used to store the spectra.

E. Data Collection and Analysis

Examples of noncoincidence and coincidence proton spectra obtained during data collection are shown in Fig. 2. The time required for a single run varied from several minutes for ^{12}C to several hours for the nickel isotopes. In the latter cases, many reactions other than

[21] Annual Report, Nuclear Physics Laboratory, University of Washington, 1960 (unpublished).
[22] Annual Report, Nuclear Physics Laboratory, University of Washington, 1966 (unpublished).
[23] C. W. Williams and J. A. Biggerstaff, Nucl. Instr. Methods 25, 370 (1964).

the one of interest occur which result in large numbers of neutrons and γ rays subsequently detected in the γ-ray detector. To prevent large gain changes and deadtime losses in the γ-ray counter, a rate of 30 000 counts/sec could not be exceeded. Run durations, therefore, could not be decreased by increasing the beam intensity.

During the course of each run, the photomultiplier gain was carefully monitored since, in order to compute the spin-flip probability, it is necessary to know the fraction of the total γ-ray spectrum contained in the pulses exceeding the energy discriminator threshold.

Simultaneous storage of noncoincidence and coincidence spectra enabled us to monitor the number of accidental coincidence events. The coincidence spectrum in Fig. 2 shows an elastic proton peak, and all counts in that peak are obviously accidental in origin. Since the probability that an elastically scattered proton produces an accidental count is the same as that for a proton scattered inelastically, the number of accidental events in the gated inelastic proton peak is $N_{ea}(N_i/N_e)$, where N_{ea} is the number of counts in the (coincidence) elastic peak, and N_i and N_e are the number of counts in the (noncoincidence) inelastic and elastic peaks, respectively. The above analysis neglects the effects of the slow-coincidence circuit and the difference in the fast and slow γ discriminator thresholds. These effects, however, were found to be negligible.

Deadtime losses of several percent were produced by the high counting rate in the γ-ray detector. Appropriate corrections were made for these losses, as well as for those occurring in the course of pulse-height analysis of the proton pulses.

We now define the *experimentally determined* quantity N_z:

$$N_z=(8\pi/5)\,(N_{ig}/N_i)\,[f_\gamma(V_s)\,\langle\eta\Omega\rangle_\gamma]^{-1}. \quad (2)$$

The quantities N_{ig} and N_i are, respectively, the number of coincidence and noncoincidence inelastic proton counts, corrected for deadtime losses and for accidental coincidences; $f_\gamma(V_s)$ is the fraction of the pulses of the total γ-ray spectrum whose amplitudes exceed the γ-ray energy discriminator threshold V_s, and $\langle\eta\Omega\rangle_\gamma$ is the effective product of γ-detector efficiency and solid angle. The function $f_\gamma(V_s)$ and the quantity $\langle\eta\Omega\rangle_\gamma$ have been experimentally determined for γ rays with energies of interest.[24] In the limit of vanishingly small solid angle, N_z is equal to the spin-flip probability (S). However, for a γ-ray detector having a finite aperture, it is necessary to correct for contributions to the true coincidence rate arising from de-excitation γ rays from the $m=0$ and the $m=\pm2$ substates of the excited nuclei. It can be shown[25] that S lies between the limits

$$S_{\min}=N_z-\theta_0^2[\tfrac{3}{2}-(11/4)N_z] \quad (3a)$$

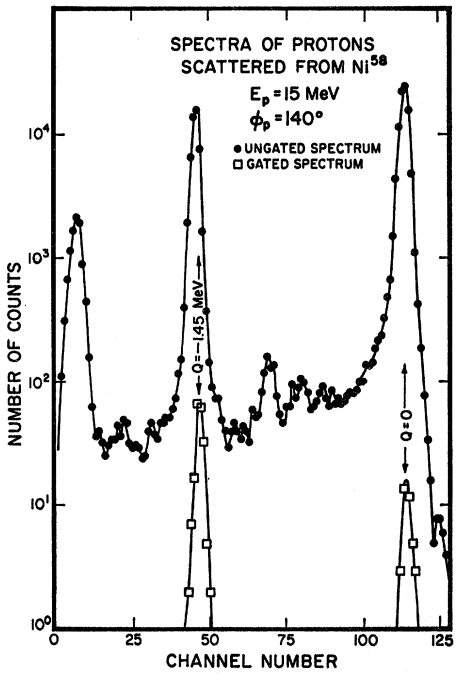

FIG. 2. Example of coincidence (gated) and noncoincidence (ungated) proton spectra accumulated during a spin-flip measurement on ^{58}Ni at 15 MeV.

and

$$S_{\max}=N_z-\theta_0^2[\tfrac{1}{2}-(7/4)N_z], \quad (3b)$$

where θ_0 is the effective half-angle of the γ-ray-detector aperture. The true value of S could be computed if the population ratio between the $m=0$ and the $m=\pm2$ substates were known. This information can be determined experimentally either by z-axis coincidence measurements with two different γ-detector acceptance angles,[26] or by measurements of the in-plane angular correlation.[4] Since we have not performed either of these measurements, we have computed S assuming equal population of the $m=0$ and $m=\pm2$ substates; that is,

$$S=N_z+\theta_0^2[(9/4)N_z-1]. \quad (4)$$

The uncertainty in S arising from the above considerations is approximately of the same magnitude as are the statistical errors in the present results.

III. RESULTS

Figure 3 shows the results of our spin-flip measurements. In each case, the spin-flip probability, computed from Eq. (4), is plotted as a function of the c.m. scattering angle. The error flags shown in the data only reflect statistical errors and do not contain the uncertainty resulting from the unknown populations of the other substates as discussed at the end of Sec. II E. The effect of this uncertainty is illustrated for the case

[24] Annual Report, Nuclear Physics Laboratory, University of Washington, 1968 (unpublished).

[25] W. A. Kolasinski, Ph.D. thesis, University of Washington, 1967 (unpublished). Note: Because of a misprint, these equations are incorrectly stated in Appendix 2 of Ref. 4.

[26] G. E. Assousa, Ph.D. thesis, Florida State University, 1968 (unpublished).

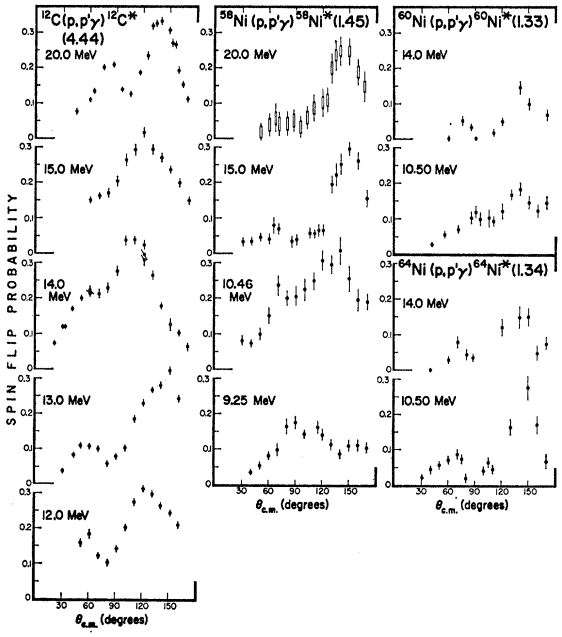

FIG. 3. Proton spin-flip probability in the reactions ^{12}C(p, p')^{12}C*(4.44), ^{58}Ni(p, p')^{58}Ni*(1.45), ^{60}Ni*(1.33), and ^{64}Ni(p, p')^{64}Ni*(1.34) at various energies.

of ^{58}Ni at 20 MeV, where the heavy bars indicate the possible values of S given by the limits in Eqs. (3).

A. Carbon

The data obtained from bombardments of ^{12}C at energies of 12–15 and 20 MeV show, in all cases, a backward peak for which the maximum spin-flip probability is about 30%. Except for the 15-MeV data, a smaller peak in the vicinity of 60°–80° can also be seen. The angular dependence of the spin-flip probability fluctuates with incident proton energy, but not nearly as drastically as was observed in the previous cyclotron runs.[4] Figure 4 shows the spin-flip excitation function on ^{12}C at 160° from 12 to 15 MeV.

B. Nickel Isotopes

In the ^{58}Ni data, we see that a change appears in the angular dependence of the spin-flip probability as the bombarding energy is increased. At 9.25 MeV, there is a broad peak at about 90°. At 10.46 MeV, the spin-flip probability peaks at approximately 130° and reaches a value of 30%. The peak is quite broad, and there is a relatively gradual decrease in magnitude toward the forward direction. The data at 15 and 20 MeV are quite similar and differ from the results at lower energy. A relatively narrow peak appears around 150° whereas below 120° the spin-flip probability is quite small.

Comparison of the ^{60}Ni data at 10.5 and at 14 MeV shows again that the spin-flip probability peaks at backward angles, with the peak becoming narrower at the higher energy. However, the magnitude of the peak is a factor of 2 lower than in ^{58}Ni.

In ^{64}Ni at 10.5 MeV, the backward peak is reminiscent of the higher-energy data in ^{58}Ni, while at 14 MeV a large decrease in its magnitude is observed. A smaller but quite pronounced peak is apparent in the vicinity of 70° at both energies.

IV. DISCUSSION

A. General Remarks

In this section we shall compare the experimental results with DWBA collective-model calculations, performed for those cases in which we believe the theory reasonably can be applied. In the case of ^{12}C, the deformation parameter β_2 for the strongly excited 2^+ level is so large that the first-order DWBA treatment cannot be expected to yield significant results, and no fits will be presented. In ^{58}Ni, the angular dependence of the spin-flip probability is observed to change with increasing proton bombarding energy from a form with a broad peak around 90° at 9.25 MeV, to one that is sharply peaked in the backward direction at 15 and 20 MeV. It has been shown by Swenson and Mohindra[27] that compound-nuclear processes contribute strongly to elastic and inelastic scattering in ^{58}Ni at proton energies around 9.5 MeV. This is not surprising, since the (p, n) threshold for ^{58}Ni is 9.3 MeV and thus there are relatively few decay channels available to the compound nucleus. On the other hand, at 15 MeV incident proton energy, many more decay channels are open, and one would expect the scattering to be predominantly direct. A study of fluctuations in proton differential scattering cross sections on ^{58}Ni, measured for incident proton energies between 14.5 and 15.5 MeV, has shown that a reasonable lower limit for the direct reaction contribution in this energy range is 85%.[24] In ^{60}Ni, where the (p, n) threshold is 6.9 MeV, we again expect compound-nuclear effects to play a significant role at incident energies below about 12 MeV.

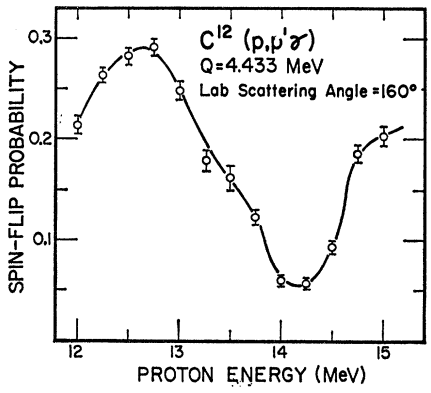

FIG. 4. Proton spin-flip probability in the reaction ^{12}C(p, p')^{12}C*(4.44) at $\phi_{lab}=160°$, as a function of incident proton energy.

[27] L. W. Swenson and R. K. Mohindra, Phys. Rev. **150**, 877 (1966).

However, the (p, n) threshold in ^{64}Ni is about 3 MeV, and hence we expect that the scattering of both 10.5 and 14 MeV protons should be predominantly direct. For the above reasons we have confined our analyses to ^{58}Ni at 15 and 20 MeV, ^{60}Ni at 14 MeV, and ^{64}Ni at 10.5 and 14 MeV.

B. Comparison of Theory with Experiment

In general, the inelastic scattering matrix element in DWBA theory is given by

$$T_{a\to b}=\langle\chi_b^{(-)}(\mathbf{k}_b, \mathbf{r}_b) \mid \langle\phi_b \mid \Delta U \mid \phi_a\rangle \mid \chi_a^{(+)}(\mathbf{k}_a, \mathbf{r}_a)\rangle, \quad (5)$$

where the ϕ's are the nuclear wave functions and the χ's are distorted waves describing the relative motion of the target and projectile and are subject to appropriate boundary conditions. ΔU is the interaction causing the inelastic event. The optical potential used to generate the χ's is of the form

$$U(r)=V_C(r)-V_0 f(r, R_0, a_0)-i[W-4a_I W_D(\partial/\partial r)] \times f(r, R_I, a_I)+(\hbar/m_\pi c)^2(V_{SO}+iW_{SO})r^{-1}(\partial/\partial r) \times f(r, R_{SO}, a_{SO})\,\boldsymbol{\sigma}\cdot\mathbf{l}, \quad (6)$$

where

$$f(r, R_k, a_k)=\{1+\exp[(r-R_k)/a_k]\}^{-1}, \qquad R_k=r_k A^{1/3}$$

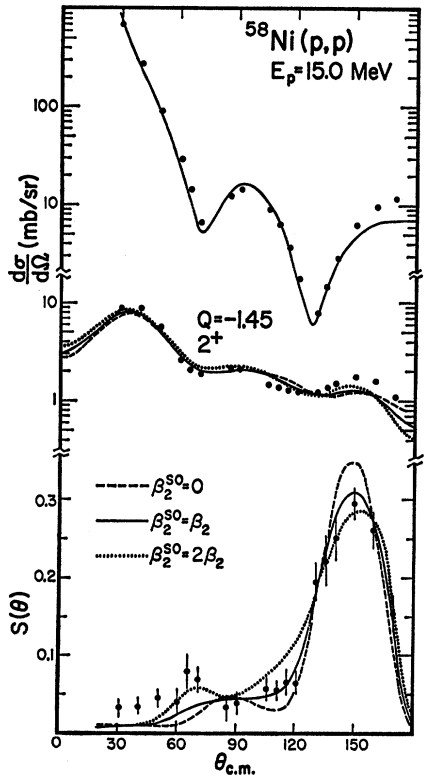

FIG. 5. Elastic and inelastic differential cross sections and spin-flip probability for ^{58}Ni at 15 MeV. The curves are optical-model (Table I parameters) and DWBA collective-model calculations with different values of β_2^{SO} for the full Thomas form of the spin-dependent interaction potential. $\beta_2=0.22$.

TABLE I. Optical-model parameters with $r_0=1.1$ F, $r_I=1.25$ F, $r_{SO}=1.00$ F, and $a_0=a_I=a_{SO}\simeq 0.7$ F.

Target	E_p (MeV)	V (MeV)	W_D (MeV)	V_{SO} (MeV)	χ^2
^{58}Ni	15.0	61.80	7.19	5.8	15.3
	20.0	59.88	6.91	5.3	15.6
^{60}Ni	14.0	60.81	7.72	3.2	18.1
^{64}Ni	10.5	65.15	7.52	6.0	3.1
	14.0	61.84	8.80	4.9	10.3

with k representing the subscripts 0, I, and SO; $V_C(r)$ = the Coulomb potential for a uniformly charged sphere of radius R_C, where $R_C=r_C A^{1/3}$. The interaction ΔU for collective excitations is obtained by deforming $U(r)$; that is, the variables $R_k'=R_k+\alpha_k(\hat{r})$ are substituted for R_k in $U(r)$, and $U(r)$ is expanded to first order in $\alpha_k(\hat{r})$ to obtain

$$\Delta U=\Delta U_0+i\Delta U_I+\Delta U_{SO}, \quad (7)$$

where

$$\Delta U_0=-\alpha_0(\hat{r})\,V_0(\partial/\partial R_0)f(r, R_0, a_0), \quad (8)$$

$$\Delta U_I=-\alpha_I[W-4a_I W_D(\partial/\partial r)](\partial/\partial R_I)f(r, R_I, a_I). \quad (9)$$

Deformation in the Coulomb potential is neglected. Following the prescription of Blair and Sherif,[14,28] the deformed spin-orbit term (ΔU_{SO}) is obtained from the Thomas form of the spin-orbit potential,

$$U_{SO}=(\hbar/m_\pi c)^2(V_{SO}+iW_{SO})\,\boldsymbol{\sigma} \cdot[\nabla f(r, R_{SO}, a_{SO})\times i^{-1}\nabla]. \quad (10)$$

Expanding to first order in $\alpha_{SO}(\hat{r})$, one obtains for the deformed part

$$\Delta U_{SO}=(\hbar/m_\pi c)^2(V_{SO}+iW_{SO})\,\boldsymbol{\sigma} \cdot\{\nabla[\alpha_{SO}(\hat{r})\,(\partial f/\partial R_{SO})]\times i^{-1}\nabla\}, \quad (11)$$

which can be written as the sum of two terms:

$$\Delta U_{SO}=\Delta U_{SO}(1)+\Delta U_{SO}(2), \quad (12)$$

where

$$\Delta U_{SO}(1)=(\hbar/m_\pi c)^2(V_{SO}+iW_{SO})\,\alpha_{SO}(\hat{r}) \times r^{-1}(\partial/\partial r)\,(\partial f/\partial R_{SO})\,\boldsymbol{\sigma}\cdot\mathbf{l}, \quad (13)$$

$$\Delta U_{SO}(2)=(\hbar/m_\pi c)^2(V_{SO}+iW_{SO})\,(\partial f/\partial R_{SO})\,\boldsymbol{\sigma} \cdot\{\nabla[\alpha_{SO}(\hat{r})]\times i^{-1}\nabla\}. \quad (14)$$

The deformation parameters $\alpha_k(\hat{r})$ are expanded in the usual way:

$$\alpha_k(\hat{r})=\sum_{lm}\alpha_{lm}{}^k R_k Y_l{}^{m*}(\hat{r}), \quad (15)$$

and the nuclear matrix elements of $\alpha_{lm}{}^k$ are parametrized by $\beta_l{}^k(2l+1)^{-1/2}$.

[28] H. Sherif, Ph.D. thesis, University of Washington, 1968 (unpublished).

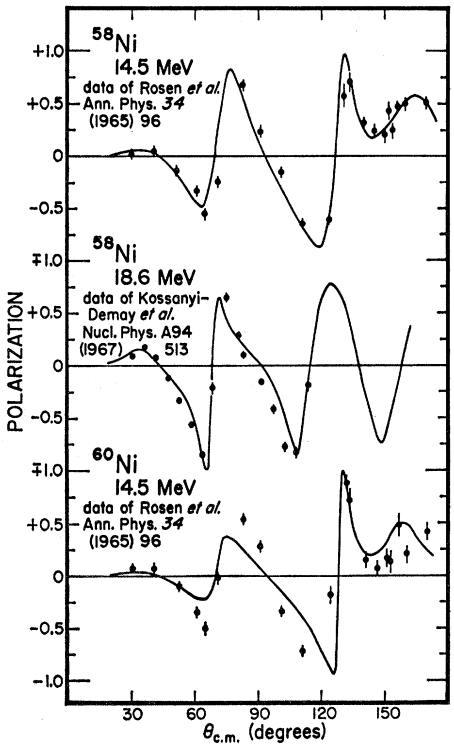

FIG. 6. Comparison of elastic polarization predictions (Table I parameters) for ^{58}Ni at 15 MeV and ^{60}Ni at 14 MeV with the experimental data of Rosen *et al.* at 14.5 MeV, and for ^{58}Ni at 20 MeV with the experimental data of Kossanyi-Demay *et al.* at 18.6 MeV.

Equations (13) and (14) embody what Sherif and Blair consider to be the full Thomas form of the spin-dependent coupling potential. The first of these equations is the unsymmetrized version of the deformed potential used by the Oak Ridge group in their calculations.[2,10] More recent analyses, however, have shown that the full Thomas form results in improved fits, for medium energy protons, for inelastic asymmetries[14,28] and spin-flip probabilities.[13,18]

Our calculations were performed on an IBM 7094 computer, with a code developed by Sherif.[28] Predictions were obtained for inelastic scattering cross sections and spin-flip probabilities with the full Thomas form of the spin-dependent coupling potential for the cases $\beta_2^{SO}=0$, $\beta_2^{SO}=\beta_2$, and $\beta_2^{SO}=2\beta_2$. Optical-model parameters were obtained with the search code ABACUS.[29] For these calculations, $W=W_{SO}=0$, $r_C=r_0$, and $a_{SO}=a_0$. No attempt was made to perform an extensive parameter search, as it was found that generally acceptable fits to the elastic cross-section data, for all cases, could be obtained with the geometrical parameters fixed at the values: $r_0=1.1$ F, $r_I=1.25$ F, $r_{SO}=1.00$ F, and $a_0=a_I=a_{SO}\simeq 0.7$ F. Searches on the depths of the potentials (V_0, W_D, and V_{SO}) revealed that the elastic cross-section predictions were relatively insensitive to changes in the depth of the spin-orbit potential (V_{SO}). On the other hand, DWBA predictions of the magnitude of the spin-flip probability have been found to be markedly sensitive to this parameter.[18] Since for all cases polarization data were not available at the energies of the present experiment, the spin-orbit potential depths were determined by an iterative procedure, which consisted of matching the DWBA predictions with the magnitudes of the back-angle peak in the measured probabilities and then again performing an optical-model search to optimize the elastic scattering cross-section fits. The resulting parameters are summarized in Table I. The values of χ^2 in the table reflect the elastic predictions only, and can be compared for goodness of fit for the different cases, as the relative experimental errors for all cases were assumed to be 5%.

The best over-all agreement with experimental data was obtained for the case of ^{58}Ni at 15 MeV (Fig. 5). Except for some discrepancy at back angles, the differential cross-section data are quite adequately reproduced by theoretical predictions. As might be expected, the inelastic cross section is generally enhanced by an increased spin-orbit deformation, but this effect is not spectacular and leaves little basis for differentiation

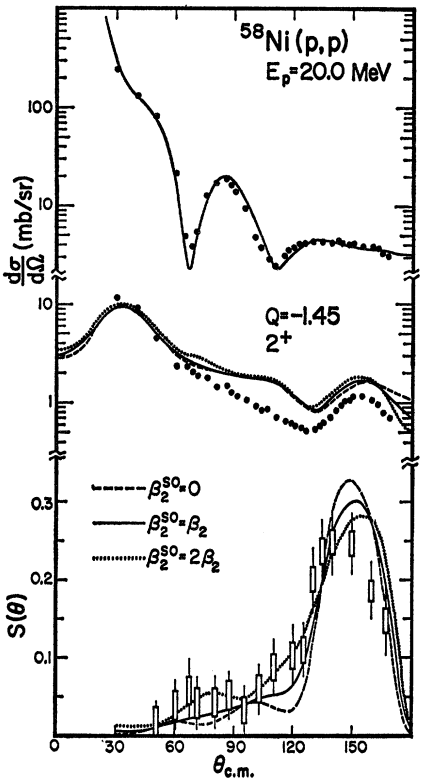

FIG. 7. Elastic and inelastic differential cross sections and spin-flip probability for ^{58}Ni at 20 MeV. The curves are optical-model (Table I parameters) and DWBA collective-model calculations with different values of β_2^{SO} for the full Thomas form of the spin-dependent interaction potential. $\beta_2=0.21$.

[29] E. H. Auerbach, ABACUS-2 (Revised Version), Brookhaven National Laboratory, 1962 (unpublished).

between the cases presented. On the other hand, the predicted spin-flip probability is markedly sensitive to the amount of spin-orbit deformation, particularly at forward angles where, for $\beta_2^{SO}=2\beta_2$, the small peak at 70° appears to be in better agreement with experiment. It is interesting to note that the predicted spin-flip probability is large, even when the spin-orbit potential is not deformed ($\beta_2^{SO}=0$), indicating that spin flip is caused predominantly by spin-orbit distortions in the elastic channel. We have also compared our predicted elastic polarization for ^{58}Ni at 15 MeV with the experimental data of Rosen *et al.*[30] at 14.5 MeV (Fig. 6) and find the fit to be quite adequate.

At 20 MeV the agreement of the theory with experiment is not as good as in the 15-MeV data, but the general trends are qualitatively reproduced (Fig. 7). There is a large discrepancy with the data in the predictions of the inelastic differential cross section at the back angles, and the predicted spin-flip probability appears to peak too far in the backward direction. The spin-flip data, in this case, are presented so as to reflect the previously mentioned uncertainty due to the finite acceptance angle of the γ-ray detector. Qualitatively,

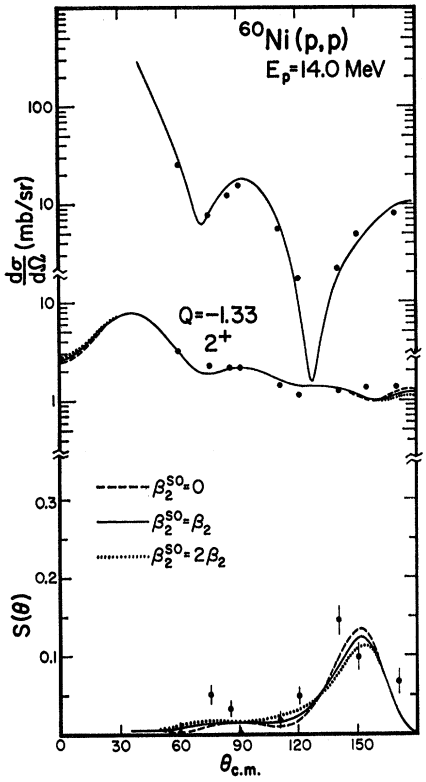

FIG. 8. Elastic and inelastic differential cross sections and spin-flip probability for ^{60}Ni at 14 MeV. The curves are optical-model (Table I parameters) and DWBA collective-model calculations with different values of β_2^{SO} for the full Thomas form of the spin-dependent interaction potential. $\beta_2=0.24$.

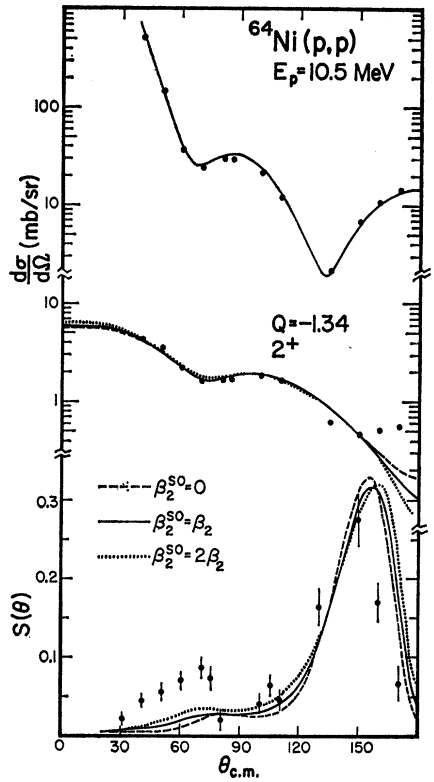

FIG. 9. Elastic and inelastic differential cross sections and spin-flip probability for ^{64}Ni at 10.5 MeV. The curves are optical-model (Table I parameters) and DWBA collective-model calculations with different values of β_2^{SO} for the full Thomas form of the spin-dependent interaction potential. $\beta_2=0.21$.

it appears that $\beta_2^{SO}>\beta_2$ gives better agreement of theory with experiment, as for the case of the 15-MeV spin-flip data, and this observation is also consistent with analyses of inelastic asymmetries[2] at higher energies. The predicted elastic polarization compares favorably with the 18.6-MeV polarization data of Kossanyi-Demay *et al.*[31] (Fig. 6).

For ^{60}Ni and ^{64}Ni (Figs. 8–10), the predictions of the DWBA theory are not as good. The ^{60}Ni data at 14 MeV are quite sketchy and the over-all normalization of the spin-flip probability is somewhat in doubt. The reduced magnitude thus constrains V_{SO} to a small value and a poor fit is obtained for the elastic polarization (Fig. 6). In ^{64}Ni, again, we have no way of reproducing the energy variation of the spin-flip probability without making a large variation in V_{SO}. The large discrepancy at forward angles is also quite apparent, and the theoretical curves put the peaks too far in the backward direction. The change with energy of the backward peak magnitude resembles the trend in the ^{66}Zn spin-flip data reported by Perey.[17] The effect of the spin-orbit deformation becomes more pronounced as the energy is increased.

[30] L. Rosen, J. G. Beery, and A. S. Goldhaber, Ann. Phys. (N.Y.) **34**, 96 (1965).

[31] P. Kossanyi-Demay, R. de Swiniarski, and C. Glashausser, Nucl. Phys. **A94**, 513 (1967).

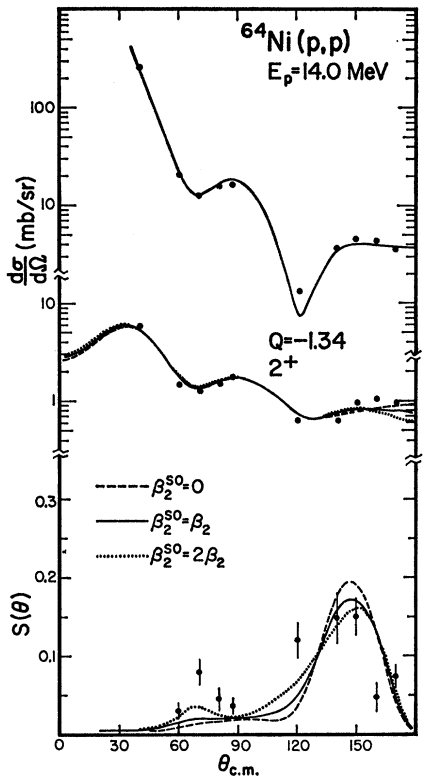

FIG. 10. Elastic and inelastic differential cross sections and spin-flip probability for ^{64}Ni at 14 MeV. The curves are optical-model (Table I parameters) and DWBA collective-model calculations with different values of β_2^{SO} for the full Thomas form of the spin-dependent interaction potential. $\beta_2=0.21$.

C. Summary and Conclusions

In conclusion we will summarize some of the observations in the measured spin-flip probabilities and corresponding analyses. The variation with energy, in which the spin-flip probability assumes an angular dependence characterized by a pronounced backward peak as the bombarding energy is increased, is observed to be a general feature of the data in all cases. This correlation suggests that, at lower energy, compound-nuclear processes play a role in proton spin flip, whereas at higher energy, the backward-peaked pattern observed may be a signature of a direct reaction process. Indeed, the higher-energy data are adequately described by the DWBA collective-model treatment, and the calculations always yield a backward-peaked pattern. Since our parameter search was by no means completely exhaustive, and we have not investigated the effects of introducing a volume-imaginary potential, an imaginary spin-orbit term or different sets of geometrical parameters for all cases, it is quite possible that a consistent set of parameters can be found to give a much better over-all account of the data. The variation with energy, and with neutron number for the nickel isotopes, in the magnitude of the spin-flip probability is as yet unexplained.

Predictions of the spin-flip probability are markedly sensitive to deformations in the spin-orbit potential, and the data is strongly suggestive of improved fits with $\beta_2^{SO}>\beta_2$. The uncertainty due to the solid angle of the γ-ray detector, however, prevents our drawing any more definite quantitative conclusions regarding the effect of introducing the spin-orbit deformation.

Finally, for a given isotope at a particular energy, the magnitude of the predicted spin-flip probability is quite sensitive to the magnitude of V_{SO}. Good fits are, in general, obtained for elastic polarization data when V_{SO} is thus determined from spin-flip data in conjunction with elastic cross-section data. The present analyses may not be conclusive in this respect, but the possibility that the depth of V_{SO} in the optical potential can be so determined is quite attractive. Acquisition of higher-precision experimental data and a more thorough theoreticial investigation are certainly warranted.

ACKNOWLEDGMENTS

We wish to thank Professor J. S. Blair for discussions and numerous helpful suggestions concerning the theoretical aspects of this work. Special thanks are due to Professor J. G. Cramer, B. Fernandez, T. D. Hayward, and D. M. Patterson for their assistance in the experimental work and collection of data. We are also grateful to Professor T. J. Morgan (deceased), H. Fauska, J. W. Orth, H. E. Bennett, Mrs. Peggy Douglass, Miss Joanne Sauer, and the other members of the staff of the University of Washington Nuclear Physics Laboratory.